Propagation of transverse intensity correlations of a two-photon state

D. S. Tasca,* S. P. Walborn, and P. H. Souto Ribeiro†
Instituto de Física, Universidade Federal do Rio de Janeiro, Caixa Postale 68528, Rio de Janeiro 21941-972, Brazil

F. Toscano
Fundação Centro de Ciências e Educação Superior a Distância do Estado do Rio de Janeiro, Rio de Janeiro 20943-001, Brazil and Instituto de Física, Universidade Federal do Rio de Janeiro, Caixa Postale 68528, Rio de Janeiro 21941-972, Brazil

P. Pellat-Finet
Groupe d'Optique Théorique et Appliquée, LMAM, Université de Bretagne Sud, BP 92116, Lorient Cedex, France and Département d'Optique, UMR CNRS 6082, École Nationale Supérieure des Télécommunications de Bretagne, CS 833813 29238 BREST cedex 3, France

(Received 22 August 2008; published 4 March 2009)

The propagation of transverse spatial correlations of photon pairs through arbitrary first-order linear optical systems is studied experimentally and theoretically using the fractional Fourier transform. Highly correlated photon pairs in an Einstein-Podolsky-Rosen-like state are produced by spontaneous parametric down-conversion and subject to optical fractional Fourier transform systems. It is shown that the joint detection probability can display either correlation, anticorrelation, or no correlation, depending on the sum of the orders α and β of the transforms of the down-converted photons. We present analytical results for the propagation of the perfectly correlated EPR state and numerical results for the propagation of the two-photon state produced from parametric down-conversion. We find good agreement between the theory and experiment.

DOI: 10.1103/PhysRevA.79.033801 PACS number(s): 42.50.Xa, 42.50.Dv, 03.65.Ud

I. INTRODUCTION

The discussion about nonlocal correlations between properties of two separated particles began in part with the famous Einstein-Podolsky-Rosen (EPR) paper [1], in which Einstein *et al.* showed that the position and momentum of two correlated particles could be used to construct a paradox between quantum theory and intuitive concepts such as locality and the reality of physical properties. Continuous-variable (CV)-entangled states similar to the EPR state appear in a number of physical systems, including field-quadrature correlations of two modes of the electromagnetic field [2–5], spatial variables of pairs of photons [6,7], and others [8–11]. This has allowed the experimental realization of the original gedanken experiment proposed by EPR [2,6,7]. CV entanglement of the EPR type has been shown to be useful for a number of quantum information tasks [12]. One of the benefits to the study and the use of CVs is the access to a Hilbert space of larger dimension, which is advantageous for quantum cryptography [13,14] and fundamental tests of quantum mechanics [15].

EPR-like spatial correlations can be identified by the violation of the inequality [16,17]

$$\Delta^2(\rho_1|\rho_2)\Delta^2(q_1|q_2) > \frac{1}{4}, \tag{1}$$

where $\Delta^2(\rho_1|\rho_2)$ represents the uncertainty in variable ρ_1 of system 1 conditioned upon measurement of system 2 at ρ_2. $\Delta^2(\rho_1|\rho_2)$ is the variance of the conditional probability $P(\rho_1|\rho_2)$ for a fixed value of ρ_2. Similarly, $\Delta^2(q_1|q_2)$ is the variance of the conditional probability $P(q_1|q_2)$, where q_1 and q_2 are the Fourier conjugate variables of ρ_1 and ρ_2. If inequality (1) is violated, one could infer either ρ_1 or q_1 from conditional measurements ρ_2 or q_2, with less uncertainty than the Heisenberg uncertainty principle would allow. In recent experiments [6,7], measurements of this type were performed in the coincidence-counting regime using photons from spontaneous parametric down-conversion (SPDC). The transverse position and momentum were determined by measuring the intensity distributions in the near and far field, respectively. As inequality (1) deals with EPR's nonlocality, it is generally more restrictive than those involving variances of center of mass and relative variables, which identify nonseparability of continuous-variable systems [18,19].

The spatial correlations of photon pairs produced by SPDC present a rich playground to investigate CV correlations with relatively simple linear optical systems [20–26]. In SPDC sources, photon pairs generally display an intensity correlation in the near field (source), due to the localized emission of the photon pair: the photons are "born" from the same pump photon so that both photons are detected at nearly the same position in the source plane. As the entangled two-photon state propagates, this spatial correlation evolves to an anticorrelation in the far field. Consequently, if photon 1 is detected at position $\boldsymbol{\rho}$ in the far field, photon 2 will be found near $-\boldsymbol{\rho}$. The far-field anticorrelations are due to the phase matching (momentum conservation) in the nonlinear SPDC interaction. The spatial correlation in the near field and anticorrelation in the far field have been previously observed in Ref. [27]. The switch from a near-field correlation to a far-field anticorrelation raises the question as to what type of correlation is present at intermediate distances in between the near and far-field regions. Recently, Chan

*tasca@if.ufrj.br
†phsr@if.ufrj.br

et al. [28] showed that the correlations can "migrate" entirely to the phase of the two-photon wave function, and consequently the conditional intensity distribution may display no correlation at all. In Ref. [29], it was shown that it is always possible to detect transverse entanglement performing only intensity correlation measurements, when an arbitrary propagation is applied to each of the entangled photons.

The propagation of the transverse spatial structure of an optical field can be accurately described by the fractional Fourier transform (FRFT) [30]. This is true for any first-order linear optical system. That includes free-space propagation alone [31–33] and also optical systems consisting of lenses and free space [30,34] provided that one chooses the appropriate scaling of the transverse coordinates. The FRFT is parametrized by an angle α so that $\alpha=0$ corresponds to an identity operation and $\alpha=\pi/2$ is the usual Fourier transform. With proper scaling of the coordinates, the FRFT is additive, so that consecutive FRFT's $\mathcal{F}_\alpha$ and $\mathcal{F}_\beta$ can be written as $\mathcal{F}_{\alpha+\beta}$. This allows one to associate an overall FRFT with an arbitrary first-order linear optical system.

In the present work, we study the transverse EPR correlations of propagating SPDC photon pairs using the FRFT. We show theoretically and experimentally that the presence of EPR intensity correlation, anticorrelation, or no correlation depends on the sum of the orders α and β of the applied FRFT transforms in each of the down-converted photons. In this way, it is possible to engineer the spatial intensity correlations through the application of optical FRFTs to the entangled down-converted photons. The FRFT describes a canonical rotation in phase space and applies to any pair of conjugate variables such as time frequency [30] or field quadratures [12]. Thus, the conclusions drawn here are also relevant to other physical systems.

In Sec. II, we review the connection between the Hilbert space associated with the spatial variables of a single- and two-photon field and the Hilbert spaces of point particles with 2 degrees of freedom. This allows us to apply the usual quantum formalism for point particles in the description of the spatial properties of single- and two-photon states. In Sec. II A, we discuss the propagation of photons through first-order linear optical systems and the use of the FRFT in this description. Section III presents the type of two-photon state typical of the SPDC process and discusses the propagation of transverse correlations under FRFT operations. In Sec. IV we present an experiment and results which are well described by the theoretical results presented in Sec. III. Finally, we provide some concluding remarks in Sec. V.

II. SINGLE- AND TWO-PHOTON STATES

Here we focus on the spatial structure of a single- or two-photon field. Thus, for simplicity, we will assume that the fields are paraxial, monochromatic, and have well-defined polarization. The Hilbert space $\mathcal{H}_1$ describing the transverse spatial degrees of freedom of a single-photon state $|\psi\rangle$ is spanned by the basis $\{|\bar{\boldsymbol{\rho}}\rangle \equiv \hat{a}^\dagger(\bar{\boldsymbol{\rho}})|0\rangle\}$, where $|0\rangle$ is the vacuum state. An arbitrary pure state is then

$$|\psi\rangle = \int d\bar{\boldsymbol{\rho}} w(\bar{\boldsymbol{\rho}})|\bar{\boldsymbol{\rho}}\rangle, \tag{2}$$

where $\bar{\boldsymbol{\rho}} \equiv (\bar{\rho}_x, \bar{\rho}_y)$ is the transverse position and $w(\bar{\boldsymbol{\rho}})$ is the transverse wave function or detection amplitude. The basis states $\{|\bar{\boldsymbol{\rho}}\rangle\}$ correspond in second quantization to unnormalized states of one photon at position $\bar{\boldsymbol{\rho}}$. It is possible to establish an isomorphism between $\mathcal{H}_1$ and the Hilbert space spanned by position eigenstates of a two-dimensional position operator $\hat{\bar{\boldsymbol{\rho}}} \equiv (\hat{\bar{\rho}}_x, \hat{\bar{\rho}}_y)$ if one specifies the action of this operator on the basis states as: $\hat{\bar{\boldsymbol{\rho}}}|\bar{\boldsymbol{\rho}}\rangle = \bar{\boldsymbol{\rho}}|\bar{\boldsymbol{\rho}}\rangle$.

Alternatively, $\mathcal{H}_1$ is spanned by the basis $\{|\bar{\mathbf{q}}\rangle \equiv \hat{a}^\dagger(\bar{\mathbf{q}})|0\rangle\}$, where

$$\hat{a}^\dagger(\bar{\mathbf{q}}) = \int d\bar{\boldsymbol{\rho}} e^{i\mathbf{p}\cdot\mathbf{q}} \hat{a}^\dagger(\bar{\boldsymbol{\rho}}) \tag{3}$$

and $\bar{\mathbf{q}} \equiv (\bar{q}_x, \bar{q}_y)$ are the transverse components of the wave vector $\mathbf{k}$. In this basis, the wave function $v(\bar{\mathbf{q}})$ is the angular spectrum of the photon field and is obtained by a Fourier transform of the detection amplitude $w(\bar{\boldsymbol{\rho}})$. Again, it is possible to establish an isomorphism between $\mathcal{H}_1$ and the space spanned by momentum eigenstates of a two-dimensional momentum operator $\hat{\bar{\mathbf{q}}} \equiv (\hat{\bar{q}}_x, \hat{\bar{q}}_y)$ if the action of this operator on the basis states is $\hat{\bar{\mathbf{q}}}|\bar{\mathbf{q}}\rangle = \bar{\mathbf{q}}|\bar{\mathbf{q}}\rangle$. Because the two bases $\{|\bar{\boldsymbol{\rho}}\rangle\}$ and $\{|\bar{\mathbf{q}}\rangle\}$ are related via a Fourier transform similar to the one in Eq. (3), the position and momentum operators satisfy the canonical commutation relations $[\hat{\bar{\rho}}_k, \hat{\bar{q}}_l] = i\delta_{k,l}\hat{\mathbb{I}}$, where $k,l=\{x,y\}$. Thus, at the level of quantum kinematics, there is an isomorphism between the Hilbert space corresponding to transverse spatial degrees of freedom of single-photon states and the Hilbert space of quantum states of a point particle with 2 degrees of freedom. The equivalence between the classical paraxial wave optics and the nonrelativistic quantum mechanics of two-dimensional point particles is well known [35] and also allows one to establish the isomorphism at the level of quantum dynamics. In fact, for paraxial propagation of the photons along an optical axis z, the wave equation that governs the evolution of the wave function $w(\bar{\boldsymbol{\rho}}) \equiv \langle\bar{\boldsymbol{\rho}}|w\rangle$ is a time-dependent Schrödinger equation where the length variable z plays the role of time, and the wavelength λ of the photons plays the role of Planck's constant [36]. The analogy between paraxial wave propagation and nonrelativistic quantum mechanics of a point particle has been well explored [30,35,37–40].

The Hilbert space describing the transverse spatial degrees of freedom of two-photon states is simply the tensor product $\mathcal{H}_1 \otimes \mathcal{H}_2$ between the Hilbert spaces of one-photon states. Thus, $\mathcal{H}_1 \otimes \mathcal{H}_2$ is isomorphic to the Hilbert space associated with two distinguishable point particles, each one with 2 degrees of freedom. We assume that the photons are distinguishable since, in principle, they could be distinguished by their longitudinal direction of propagation or their polarization. Therefore, an arbitrary two-photon pure state can be written as

$$|\Psi\rangle = \int\int d\bar{\boldsymbol{\rho}}_1 d\bar{\boldsymbol{\rho}}_2 \Psi(\bar{\boldsymbol{\rho}}_1, \bar{\boldsymbol{\rho}}_2)|\bar{\boldsymbol{\rho}}_1\rangle_1|\bar{\boldsymbol{\rho}}_2\rangle_2, \tag{4}$$

where $\Psi(\bar{\boldsymbol{\rho}}_1, \bar{\boldsymbol{\rho}}_2) = \langle\bar{\boldsymbol{\rho}}_1, \bar{\boldsymbol{\rho}}_2|\Psi\rangle$ is the normalized wave function and $|\bar{\boldsymbol{\rho}}_1\rangle_1$ and $|\bar{\boldsymbol{\rho}}_2\rangle_2$ are position eigenstates for photons 1 and 2, respectively. Here it is assumed that the paraxial approximation has been applied along two distinct z axes, one for each single-photon field.

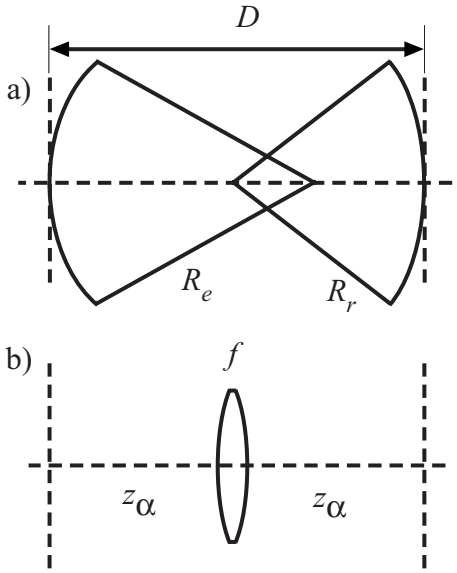

FIG. 1. (a) In free diffraction, the field on the curved surface with radius R_r can be described as the FRFT of the field on surface of radius R_e with properly scaled coordinates. (b) The FRFT can be implemented with a simple lens symmetrical system [34].

A. Propagation as a fractional Fourier transform

The most common optical systems are first-order linear systems (also called quadratic-phase systems), which are composed essentially of sections of free space and thin lenses centered on the propagation (z) axis [30]. Paraxial propagation in these systems is particularly simple. The paraxial wave equation corresponds to a Schrödinger equation associated with a quadratic Hamiltonian, so that the evolution of the phase-space operators is simply given by $(\hat{\boldsymbol{\rho}},\hat{\mathbf{q}})^{\mathbf{T}}=\hat{U}^{\dagger}(\hat{\boldsymbol{\rho}},\hat{\mathbf{q}})^{\mathbf{T}}\hat{U}=M(\hat{\boldsymbol{\rho}},\hat{\mathbf{q}})^{\mathbf{T}}$ (where $\hat{U}$ is the evolution operator associated with the quadratic Hamiltonian, and T means transposition). The symplectic matrix M is the ray matrix that stems from geometrical optics applied to the system. For example, in the case of only free propagation, the evolution is associated with the Hamiltonian of a free particle and the matrix M represents a linear canonical transformation that corresponds to a shear in the direction of the transverse momentum [30].

A great simplification and systematization in the description of evolution through first-order optical systems is gained by using dimensionless variables $\boldsymbol{\rho}=\bar{\boldsymbol{\rho}}/s$ and $\bar{\mathbf{q}}=s\mathbf{q}$, where the real number s has the dimension of a length, and is generally a function of the properties of the physical system. In this case, free-space propagation can be described in the paraxial approximation with the help of the FRFT [30,32,33]. This is due to the fact that the paraxial Fresnel diffraction integral, which relates the light signal between two transverse planes in free space, can be expressed using a FRFT if we use dimensionless coordinates. The more general case occurs when we choose different parameters s at the input and the output planes. However, in order to identify the transverse position and momentum coordinates at these planes as belonging to the same phase space, one must use the same parameter s. Figure 1(a) illustrates the identification of the FRFT with propagation through free space. The diffraction of light from a spherical cap emitter with radius of curvature $R_e=-R<0$ to a spherical cap receiver with radius of curvature $R_r=R>0$ at a distance z from the emitter can be expressed as [32,33]

$$\phi_r(\boldsymbol{\rho}) = e^{-i\alpha/2}\mathcal{F}_{\alpha}[\phi_e(\boldsymbol{\rho})], \tag{5}$$

where $\phi_e(\boldsymbol{\rho})=\exp(-ik|s\rho|^2/2R_e)\varphi_e(\boldsymbol{\rho})$ and $\phi_r(\boldsymbol{\rho})=\exp(-ik|s\rho|^2/2R_r)\varphi_r(\boldsymbol{\rho})(k\equiv|\mathbf{k}|=2\pi/\lambda)$. $\varphi_e(\boldsymbol{\rho})$ and $\varphi_r(\boldsymbol{\rho})$ are the wave functions at the planes of observations tangent to the emitter's and receiver's spherical caps at its vertex point. Here we call the angle $0<\alpha<\pi$ the order of the FRFT. This order $\alpha\equiv\alpha(R,z)$ and the adimensionalization parameter $s\equiv s(R,z)$ can be calculated from the relations $s=\sqrt{z/k}(1-g^2)^{-1/4}$ and $g\equiv 1-z/R=\cos\alpha$. Alternatively, given the parameter s and the distance z, we can estimate the FRFT's order $\alpha\equiv\alpha(s,z)$ and the radius of curvature $R\equiv R(s,z)$. It is important to note that the quadratic phase factors that map the wave functions at the spherical caps to the wave functions at their tangent planes are not important if we are concerned only with intensity measurements at these planes.

The description of the propagation of photons through first-order optical systems with the help of the FRFT is completed if we use Eq. (5) in the section of free propagation, and for the action of thin lens we multiply the wave function at the plane of the lens by the phase factor $\exp(-ik|s\rho|^2/2f)$, where f is the focal length of the lens. It is important to maintain the same dimensionless parameter s along the entire optical system in order to use the additivity property $\mathcal{F}_{\alpha+\beta}=\mathcal{F}_{\alpha}\circ\mathcal{F}_{\beta}$ of the FRFT. This is the mechanism behind the implementation of a FRFT between two planar surfaces with the optical systems reported in [34], where $\varphi_r(\boldsymbol{\rho})=\mathcal{F}_{\alpha}[\varphi_e(\boldsymbol{\rho})]$. In the experiment reported in Sec. IV, we perform FRFT's using the "type I" symmetric lens system configuration, which is illustrated in Fig. 1(b). This FRFT system was originally reported in [34] and is also discussed in detail in [30]. This FRFT system consists of a lens of focal length f placed symmetrically between the input and output planes at a distance z_α from each. One can apply either Fourier optics or geometric optics to verify that this system corresponds to a FRFT. Specifically, it is necessary to define the fractional focal length $f'=f\sin\alpha$ and impose that the focal length f and the distance of propagation z_α before and after the lens are related to the order α of the FRFT via the relation $z_\alpha=2f\sin^2(\alpha/2)$. The dimensionless position and momentum coordinates for this kind of system are $\boldsymbol{\rho}=\sqrt{k/f'}\bar{\boldsymbol{\rho}}$ and $\mathbf{q}=\sqrt{f'/k}\bar{\mathbf{q}}$, where $\bar{\boldsymbol{\rho}}$ and $\bar{\mathbf{q}}$ are the dimensional variables. In operator formalism, the evolution with a FRFT is associated with the fractional Fourier operator defined as [30]

$$\hat{\mathcal{F}}_{\alpha} \equiv e^{i\alpha/2}\exp\left(-i\alpha\frac{\hat{\boldsymbol{\rho}}^2+\hat{\mathbf{q}}^2}{2}\right), \tag{6}$$

where $\hat{\boldsymbol{\rho}}$ and $\hat{\mathbf{q}}$ are the dimensionless position and momentum operators. This operator is equivalent to the evolution operator of the quantum harmonic oscillator, with the Hamiltonian defined as $\mathsf{H}=(\hat{\boldsymbol{\rho}}^2+\hat{\mathbf{q}}^2)/2$. Under the FRFT operator of order α, the single-photon state $|\varphi_0\rangle$ evolves to $|\varphi_\alpha\rangle$

$=\hat{\mathcal{F}}_\alpha|\varphi_0\rangle$. The FRFT of the wave function $\varphi_\alpha(\boldsymbol{\rho})=\langle\boldsymbol{\rho}|\varphi_\alpha\rangle$ is then given by [32]

$$\varphi_\alpha(\boldsymbol{\rho}) = \int d\boldsymbol{\rho}'\langle\boldsymbol{\rho}|\hat{\mathcal{F}}_\alpha|\boldsymbol{\rho}'\rangle\varphi_0(\boldsymbol{\rho}'), \tag{7}$$

where the kernel is

$$\langle\boldsymbol{\rho}|\hat{\mathcal{F}}_\alpha|\boldsymbol{\rho}'\rangle \equiv A_\alpha \exp\left(i\frac{\cot\alpha}{2}\rho'^2\right) \times\exp\left(i\frac{\cot\alpha}{2}\rho^2\right)\exp\left(-i\frac{\boldsymbol{\rho}\cdot\boldsymbol{\rho}'}{\sin\alpha}\right), \tag{8}$$

for $0<|\alpha|<\pi$. Here $A_\alpha=-i\exp(i\alpha/2)/(2\pi|\sin\alpha|)$. Taking the limit $\alpha\to 0$ (or $\alpha\to 2\pi$), one can show that $\langle\boldsymbol{\rho}|\hat{\mathcal{F}}_\alpha|\boldsymbol{\rho}'\rangle = \delta(\boldsymbol{\rho}-\boldsymbol{\rho}')$ and similarly $\langle\boldsymbol{\rho}|\hat{\mathcal{F}}_\alpha|\boldsymbol{\rho}'\rangle=\delta(\boldsymbol{\rho}+\boldsymbol{\rho}')$ for $\alpha\to\pm\pi$ [30]. When $\alpha=\pi/2$, the FRFT reduces to the common Fourier transform. When α does not lie in the interval $0<|\alpha|<\pi$, Eq. (8) accurately represents the FRFT kernel provided one replaces α with its value modulo 2π. The transverse position and wave-vector operators evolved under the action of FRFT are

$$\begin{pmatrix}\hat{\boldsymbol{\rho}}_\alpha\\ \hat{\mathbf{q}}_\alpha\end{pmatrix} = \hat{\mathcal{F}}_\alpha^\dagger\begin{pmatrix}\hat{\boldsymbol{\rho}}\\ \hat{\mathbf{q}}\end{pmatrix}\hat{\mathcal{F}}_\alpha = \begin{pmatrix}\cos\alpha & \sin\alpha\\ -\sin\alpha & \cos\alpha\end{pmatrix}\begin{pmatrix}\hat{\boldsymbol{\rho}}\\ \hat{\mathbf{q}}\end{pmatrix}, \tag{9}$$

which illustrates the fact that $\hat{\mathcal{F}}_\alpha$ corresponds to the rotation of angle α in phase space [30,34].

III. ENTANGLED TWO-PHOTON STATE

Let us consider now a pure two-photon state whose wave function in dimensionless coordinates is of the form

$$\Psi(\boldsymbol{\rho}_1,\boldsymbol{\rho}_2) = f(\boldsymbol{\rho}_1+\boldsymbol{\rho}_2)g(\boldsymbol{\rho}_1-\boldsymbol{\rho}_2). \tag{10}$$

This state is generally correlated provided that $f(\boldsymbol{\rho})$ and $g(\boldsymbol{\rho})$ are not identical Gaussian functions. Here it is assumed that f and g are normalized with respect to $\boldsymbol{\rho}_1$ and $\boldsymbol{\rho}_2$. The state (10) can be readily produced in a number of physical processes [11,41]. It is representative of the two-photon state at the face of the SPDC crystal, for example, provided that the pump and down-converted fields are polarized and nearly monochromatic [42]. In this case f is given by the spatial profile of the pump field and g is the Fourier transform of the phase matching function $G(\mathbf{q})=\sqrt{2L/K\pi^2}\mathrm{sinc}(L|\mathbf{q}|^2/4K)$ [43], where K is the wave number of the pump beam. In many experimental situations, $G(\mathbf{q})$ and $g(\boldsymbol{\rho})$ can be approximated by the Gaussian functions. In this case, assuming that the pump laser has a Gaussian profile, the position space wave function takes the form

$$\Psi(\boldsymbol{\rho}_1,\boldsymbol{\rho}_2) = \frac{1}{\pi\sigma_-\sigma_+}\exp\left[-\frac{|\boldsymbol{\rho}_1+\boldsymbol{\rho}_2|^2}{4\sigma_+^2}\right]\exp\left[-\frac{|\boldsymbol{\rho}_1-\boldsymbol{\rho}_2|^2}{4\sigma_-^2}\right]. \tag{11}$$

Equation (11) describes the field at the crystal face. In transverse wave-vector space, the wave function is

$$\Psi(\mathbf{q}_1,\mathbf{q}_2) = \frac{\sigma_+\sigma_-}{\pi}\exp\left[-\frac{\sigma_+^2}{4}|\mathbf{q}_1+\mathbf{q}_2|^2\right]\exp\left[-\frac{\sigma_-^2}{4}|\mathbf{q}_1-\mathbf{q}_2|^2\right], \tag{12}$$

which is obtained by taking the Fourier transform of the wave function (11). Now let us suppose that $\sigma_-\ll\sigma_+$, so that the photons exhibit a position correlation and a momentum anticorrelation. This is indeed what is generally produced in SPDC, in which it is not unusual to have $\sigma_-\sim\sigma_+/100$.

A. Propagation of transverse correlations

As discussed above, the propagation of the down-converted fields can generally be described by a FRFT operation. Let us assume that photon 1 propagates according to an α-order FRFT along axis z_1 and photon 2 according to a β-order FRFT along axis z_2. The state $|\Psi\rangle$ after propagation is given by

$$|\Psi_{\alpha,\beta}\rangle = \hat{\mathcal{F}}_\alpha^{(1)}\otimes\hat{\mathcal{F}}_\beta^{(2)}|\Psi\rangle. \tag{13}$$

The two-photon wave function then becomes $\Psi_{\alpha,\beta}(\boldsymbol{\rho}_1,\boldsymbol{\rho}_2) =\langle\boldsymbol{\rho}_1,\boldsymbol{\rho}_2|\Psi_{\alpha,\beta}\rangle$, where

$$\Psi_{\alpha,\beta}(\boldsymbol{\rho}_1,\boldsymbol{\rho}_2) = \int\int d\boldsymbol{\rho}_1' d\boldsymbol{\rho}_2'\langle\boldsymbol{\rho}_1|\hat{\mathcal{F}}_\alpha|\boldsymbol{\rho}_1'\rangle \times\langle\boldsymbol{\rho}_2|\hat{\mathcal{F}}_\beta|\boldsymbol{\rho}_2'\rangle\Psi(\boldsymbol{\rho}_1',\boldsymbol{\rho}_2'), \tag{14}$$

and the kernels are defined in Eq. (8). To get a sense of the action of the FRFT's, let us consider the limiting case of an EPR state, for which $f(\boldsymbol{\rho})\sim$ constant and $g(\boldsymbol{\rho})\sim\delta(\boldsymbol{\rho})$, giving $\Psi(\boldsymbol{\rho}_1,\boldsymbol{\rho}_2)=\delta(\boldsymbol{\rho}_1-\boldsymbol{\rho}_2)$. This situation is approximated by the state produced by SPDC when the pump beam can be treated as a plane wave. The EPR state is

$$|\Psi^{\mathrm{EPR}}\rangle = \int\int d\boldsymbol{\rho}_1 d\boldsymbol{\rho}_2\delta(\boldsymbol{\rho}_1-\boldsymbol{\rho}_2)|\boldsymbol{\rho}_1\rangle_1|\boldsymbol{\rho}_2\rangle_2, \tag{15}$$

which presents a perfect correlation, since detection of photon 2 at position $\boldsymbol{\rho}$ projects photon 1 onto a position eigenstate $|\boldsymbol{\rho}\rangle$. After FRFTs, the wave function $\Psi_{\alpha,\beta}^{\mathrm{EPR}}$ is

$$\Psi_{\alpha,\beta}^{\mathrm{EPR}}(\boldsymbol{\rho}_1,\boldsymbol{\rho}_2) = A_\alpha A_\beta\exp\left(i\frac{\cot\alpha\rho_1^2+\cot\beta\rho_2^2}{2}\right)\int d\boldsymbol{\rho} \times\exp\left(i\frac{\cot\alpha\rho^2}{2}\right)\exp\left(i\frac{\cot\beta\rho^2}{2}\right) \times\exp\left[-i\boldsymbol{\rho}\cdot\left(\frac{\boldsymbol{\rho}_1}{\sin\alpha}+\frac{\boldsymbol{\rho}_2}{\sin\beta}\right)\right]. \tag{16}$$

Performing the integral, we have

$$\Psi_{\alpha,\beta}^{\mathrm{EPR}}(\boldsymbol{\rho}_1,\boldsymbol{\rho}_2) = A_{\alpha+\beta}\exp\left[i\frac{\cot(\alpha+\beta)}{2}(\rho_1^2+\rho_2^2)\right] \times\exp\left[-i\frac{\boldsymbol{\rho}_1\cdot\boldsymbol{\rho}_2}{\sin(\alpha+\beta)}\right], \tag{17}$$

which is the kernel of an FRFT of order $\alpha+\beta$ corresponding to the propagation from an input plane (e.g., $\boldsymbol{\rho}_1$) to an output plane (e.g., $\boldsymbol{\rho}_2$). The state $|\Psi_{\alpha,\beta}^{\mathrm{EPR}}\rangle$ is then

$$|\Psi_{\alpha,\beta}^{\mathrm{EPR}}\rangle = A_{\alpha+\beta}\int\int d\boldsymbol{\rho}_1 d\boldsymbol{\rho}_2 \exp\left[i\frac{\cot(\alpha+\beta)}{2}(\rho_1^2+\rho_2^2)\right] \times\exp\left[-i\frac{\boldsymbol{\rho}_1\cdot\boldsymbol{\rho}_2}{\sin(\alpha+\beta)}\right]|\boldsymbol{\rho}_1\rangle_1|\boldsymbol{\rho}_2\rangle_2. \quad (18)$$

Using the definition of the FRFT kernel (8), we note that whenever $\alpha+\beta=0(\mathrm{mod}\,2\pi)$, the original state (15) is recovered. That is, the EPR state (15) is an eigenstate of operators of the type $\hat{\mathcal{F}}_\alpha\hat{\mathcal{F}}_{2\pi-\alpha}$, $\hat{\mathcal{F}}_\alpha\hat{\mathcal{F}}_{4\pi-\alpha}$, etc. When $\alpha+\beta=\pi(\mathrm{mod}\,2\pi)$, the correlated EPR state (15) evolves to an anticorrelated EPR state

$$|\Phi^{\mathrm{EPR}}\rangle = \int\int d\boldsymbol{\rho}_1 d\boldsymbol{\rho}_2 \delta(\boldsymbol{\rho}_1+\boldsymbol{\rho}_2)|\boldsymbol{\rho}_1\rangle_1|\boldsymbol{\rho}_2\rangle_2. \quad (19)$$

In this case, the detection of photon 2 at $\boldsymbol{\rho}$ projects photon 1 onto the state $|-\boldsymbol{\rho}\rangle$. Given any propagation characterized by an FRFT $\mathcal{F}_\alpha$ on photon 1, one can find a transformation $\mathcal{F}_\beta$ on photon 2 such that a correlation or anticorrelation is recovered. When $\alpha+\beta=\pi/2(\mathrm{mod}\,2\pi)$, this state becomes

$$|\Omega\rangle = \int d\boldsymbol{\rho}|\boldsymbol{\rho}\rangle_1|\mathbf{q}(\boldsymbol{\rho})\rangle_2, \quad (20)$$

where $|\mathbf{q}(\boldsymbol{\rho})\rangle \propto \int d\boldsymbol{\rho}' \exp[i\mathbf{q}(\boldsymbol{\rho})\cdot\boldsymbol{\rho}']|\boldsymbol{\rho}'\rangle$ is the momentum eigenstate conjugate to $|\boldsymbol{\rho}\rangle$. State (20) presents no intensity correlation. An equivalent result is found for $\alpha+\beta=3\pi/2(\mathrm{mod}\,2\pi)$. We note that the conditions for correlation, anticorrelation, and no correlation depend on the sum of the FRFT angles of the down-converted fields and not the individual angles α and β.

This simple picture drawn for the ideal EPR state is followed approximately by the two-photon state in Eq. (11). For simplicity, let us use the fact that the two-photon wave function is factorable in x and y variables: $\Psi(\boldsymbol{\rho}_1,\boldsymbol{\rho}_2)=\xi(\rho_{x_1},\rho_{x_2})\xi(\rho_{y_1},\rho_{y_2})$. Then we can consider one spatial dimension ρ for each down-converted field. Figures 2 and 3 show that the initial state (11) propagated under different FRFT's using $\sigma_+=4.076$ and $\sigma_-=0.067$. Figure 2 shows two examples of strong correlations between photons 1 and 2 when the FRFT orders satisfy the condition $\alpha+\beta=0(\mathrm{mod}\,2\pi)$ and two examples of strong anticorrelations when the condition is $\alpha+\beta=\pi(\mathrm{mod}\,2\pi)$. For the condition $\alpha+\beta=3\pi/2$, Fig. 3 shows a significant decrease in intensity correlations, although in general they do not completely disappear as is the case shown in Eq. (20) for the ideal EPR state. In fact, analytical calculation shows that, in order to have no intensity correlation, i.e., $|\langle\boldsymbol{\rho}_1,\boldsymbol{\rho}_2|\Psi_{\alpha,\beta}\rangle|^2=f_1(\boldsymbol{\rho}_1)f_2(\boldsymbol{\rho}_2)$, the exact relation between α and β is

$$\tan\alpha\tan\beta=\sigma_-^2\sigma_+^2. \quad (21)$$

Equation (21) is satisfied by FRFT orders such that $\alpha+\beta=\pi/2(\mathrm{mod}\,2\pi)$ or $\alpha+\beta=3\pi/2(\mathrm{mod}\,2\pi)$ only when $\sigma_-=1/\sigma_+$. Nevertheless, the intensity correlations present in the state Eq. (11) propagate in a fashion similar to the idealized case of the EPR state.

In the laboratory, one has access to the joint detection probability, which in the case of a two-photon state corresponds to the fourth-order correlation function [44]

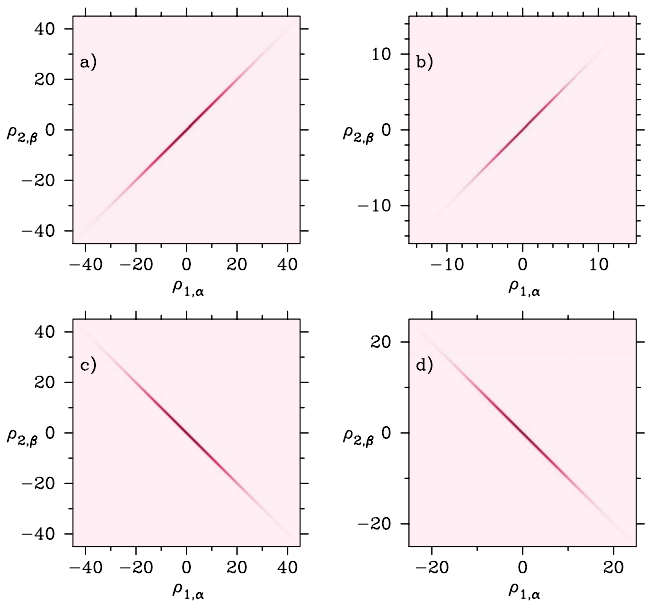

FIG. 2. (Color online) Density plot of the joint detection probability calculated for the initial Gaussian state in Eq. (11) evolved with the following FRFT orders: (a) $\alpha=3\pi/4$ and $\beta=5\pi/4$; (b) $\alpha=\pi$ and $\beta=\pi$; (c) $\alpha=\pi/4$ and $\beta=3\pi/4$; and (d) $\alpha=\pi/2$ and $\beta=\pi/2$. [Plots (a) and (b)] A strong correlation is present when $\alpha+\beta=0(\mathrm{mod}\,2\pi)$ and [plots (c) and (d)] a strong anticorrelation when $\alpha+\beta=\pi(\mathrm{mod}\,2\pi)$.

$$P_{\alpha,\beta}(\boldsymbol{\rho}_1,\boldsymbol{\rho}_2) = \langle\Psi_{\alpha,\beta}|\mathsf{a}^\dagger(\boldsymbol{\rho}_1)\mathsf{a}^\dagger(\boldsymbol{\rho}_2)\mathsf{a}(\boldsymbol{\rho}_1)\mathsf{a}(\boldsymbol{\rho}_2)|\Psi_{\alpha,\beta}\rangle = |\Psi_{\alpha,\beta}(\boldsymbol{\rho}_1,\boldsymbol{\rho}_2)|^2, \quad (22)$$

and is proportional to the number of coincidence counts $C_{\alpha,\beta}(\boldsymbol{\rho}_1,\boldsymbol{\rho}_2)$. The conditional probability can be obtained by the relation

$$P_{\alpha,\beta}(\boldsymbol{\rho}_2|\boldsymbol{\rho}_1) = \frac{P_{\alpha,\beta}(\boldsymbol{\rho}_1,\boldsymbol{\rho}_2)}{P_\beta(\boldsymbol{\rho}_1)}, \quad (23)$$

where $P_\beta(\boldsymbol{\rho}_1)$ is proportional to the number of single counts $C_\beta(\boldsymbol{\rho}_1)$. Thus, the conditional probability $P_{\alpha,\beta}(\boldsymbol{\rho}_2|\boldsymbol{\rho}_1)$ is also proportional to the number of two-photon coincidence counts $C_{\alpha,\beta}(\boldsymbol{\rho}_1,\boldsymbol{\rho}_2)$.

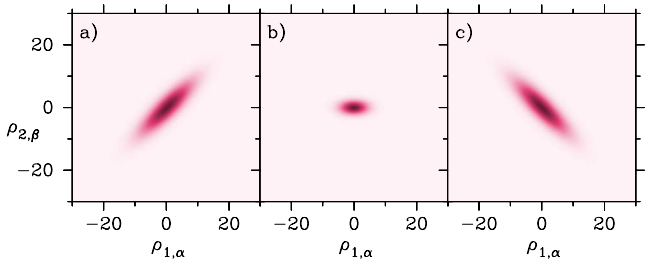

FIG. 3. (Color online) Density plot of the joint detection probability calculated for the initial Gaussian state in Eq. (11) evolved with the following FRFT orders: (a) $\alpha=\pi/4$ and $\beta=5\pi/4$; (b) $\alpha=\pi/2$ and $\beta=\pi$; and (c) $\alpha=3\pi/4$ and $\beta=3\pi/4$. In this case, with $\alpha+\beta=3\pi/2(\mathrm{mod}\,2\pi)$, we have a strong decrease in the correlations.

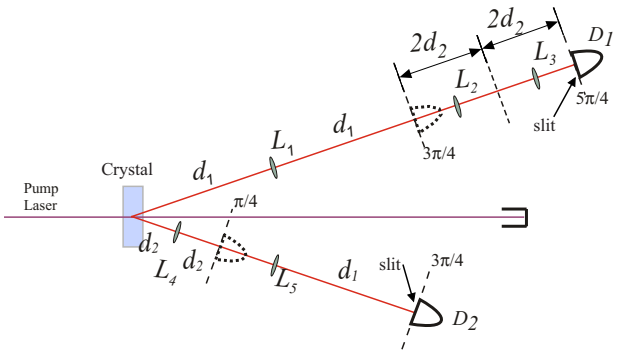

FIG. 4. (Color online) Experimental setup. The distances of the FRFT lens systems are $d_1=42.63$ cm and $d_2=7.33$ cm. All lenses have focal length $f=25$ cm. Movable slits (not shown) are placed in front of each detector.

IV. EXPERIMENT

We investigated the propagation of EPR-like correlations experimentally by implementing several FRFT's on pairs of entangled photons and registering the coincidence counts while scanning one of the detectors. The experimental setup is shown in Fig. 4. Degenerate twin photons with $\lambda=810$ nm are generated by pumping a 5-mm-long lithium iodate crystal ($LiIO_3$) with a 10-mW cw diode laser centered at $\lambda_p=405$ nm. The transverse waist of the beam at the laser output was measured to be 0.31 ± 0.01 mm. To increase the spatial correlations, the beam width is expanded three times using two confocal lenses. The down-converted photons are detected by avalanche photodiode (APD) photodetectors equipped with 10-nm bandwidth interference filters centered at 810 nm. Movable horizontal slits (3 mm$\times$100 μm) are placed directly in front of each detector in order to scan the vertical position. The FRFT's are performed on both down-converted fields using the "type I" symmetric lens system configuration reported in [34] and shown in Fig. 1(b). The dimensionless position and momentum coordinates for this kind of system are $\boldsymbol{\rho}=\sqrt{k/f'}\,\overline{\boldsymbol{\rho}}$ and $\mathbf{q}=\sqrt{f'/k}\,\overline{\mathbf{q}}$, where $f'=25/\sqrt{2}$ cm (see below) is the scaled focal length and $\overline{\boldsymbol{\rho}}$ and $\overline{\mathbf{q}}$ are the dimensional variables.

Initially, correlation measurements for the near-field ($\alpha=\beta=\pi$) and far-field ($\alpha=\beta=\pi/2$) correlations were obtained by fixing one detector at $\rho=0$ and scanning the other [6,27]. These correlations correspond to the usual position and wave-vector variables in the source plane. The near-field correlations were obtained by imaging the exit surface of the crystal on the plane of the detectors with $4f$ lens systems. For the far-field measurements, the usual optical Fourier transform system was used. A sample of the coincidence counts is shown in Fig. 5, as a function of the dimensionless variable ρ_2. The conditional variances are listed in Table I. Using these results, we can evaluate the EPR inequality (1),

$$\Delta^2_{\pi,\pi}(\rho_1|\rho_2)\Delta^2_{\pi,\pi}(q_1|q_2)=0.20\pm0.01<\frac{1}{4}, \tag{24}$$

$$\Delta^2_{\pi,\pi}(\rho_2|\rho_1)\Delta^2_{\pi,\pi}(q_2|q_1)=0.14\pm0.01<\frac{1}{4}, \tag{25}$$

which shows that the state displays nonlocal correlations. Also shown in Fig. 5 are the results using different lens configurations, which give the weakly correlated intensity distributions. For example, the $\pi-\pi/2$ distribution is more than ten times larger than the $\pi-\pi$ and $\pi/2-\pi/2$ distributions.

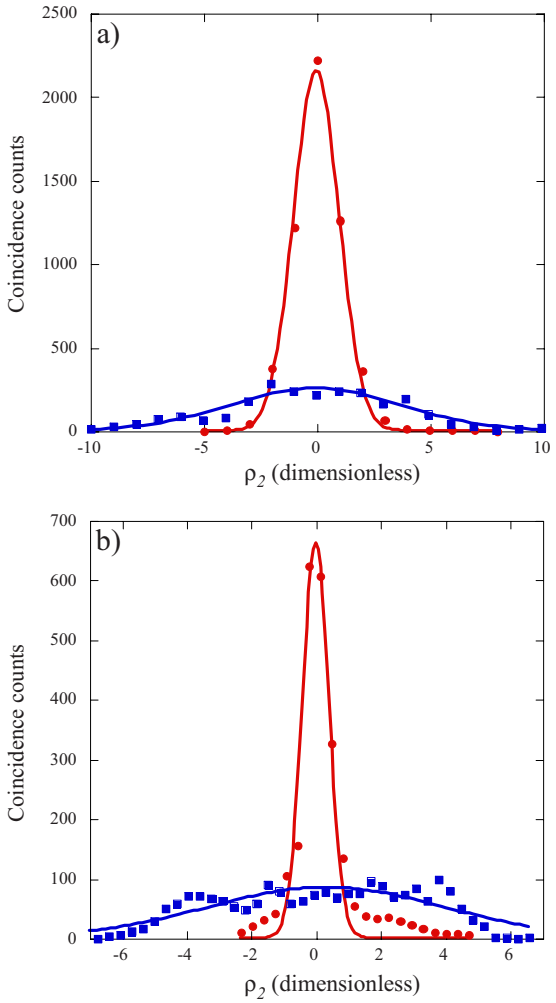

FIG. 5. (Color online) Coincidence counts $C_{\alpha,\beta}(\rho_1,\rho_2)$ as a function of dimensionless ρ_2 for (a) $\alpha=\pi,\beta=\pi$ (red circles) and $\alpha=\pi/2,\beta=\pi$ (blue squares) and (b) $\alpha=\pi/2,\beta=\pi/2$ (red circles) and $\alpha=\pi,\beta=\pi/2$ (blue squares). In all cases, detector 1 is fixed at $\rho_1=0$.

TABLE I. Conditional variances for all measurement results for different FRFT orders α and β. Variances were obtained from Gaussian curve fits.

α,β	$\Delta^2_{\alpha,\beta}(\rho_2\|\rho_1)$	$\Delta^2_{\alpha,\beta}(\rho_1\|\rho_2)$
$\alpha=\pi/2,\beta=\pi/2$	0.14 ± 0.02	0.17 ± 0.02
$\alpha=\pi,\beta=\pi$	0.98 ± 0.06	1.39 ± 0.06
$\alpha=\pi/2,\beta=\pi$	12.3 ± 1.5	
$\alpha=\pi,\beta=\pi/2$	13.3 ± 2.1	
$\alpha=3\pi/4,\beta=5\pi/4$	0.29 ± 0.01	0.28 ± 0.02
$\alpha=\pi/4,\beta=3\pi/4$	0.21 ± 0.01	0.31 ± 0.02
$\alpha=\pi/4,\beta=5\pi/4$	9.2 ± 0.7	13.8 ± 1.2
$\alpha=3\pi/4,\beta=3\pi/4$	12.1 ± 1.1	17.7 ± 1.1

To evaluate the strength of these correlations under different FRFTs, a series of measurements was performed with various FRFT lens systems. All the lenses used in the experimental setup have the same focal length $f=25$ cm. We chose FRFT's with orders $\alpha=\{\frac{3\pi}{4},\frac{5\pi}{4}\}$ and $\beta=\{\frac{\pi}{4},\frac{3\pi}{4}\}$, where α and β correspond to photons 1 and 2, respectively. These FRFT orders sum to either π, $3\pi/2$, or 2π. This choice of angles is especially convenient, as it maintains $f'=25/\sqrt{2}$ cm; the same for all of the FRFT systems used. This is advantageous for several reasons: (i) to respect the condition of additivity of two consecutive FRFT's systems and (ii) to use the same scaling factor for signal and idler fields which is necessary in order to describe the FRFT mathematically as a rotation in phase space. The scaling parameter for our system is $\sqrt{k/f'}=6.62$ mm^{-1}.

The various lenses used to implement these FRFTs are shown in Fig. 4. Three additive FRFT lens systems were used to perform the $5\pi/4$ order FRFT. Lens L_1 is used to perform a $3\pi/4$ order FRFT of the field from the exit face of the crystal to position $2d_1$. Lenses L_2 and L_3 each performs a $\pi/4$ order FRFT; the first from $z=2d_1$ to $z=2d_1+2d_2$ and the second from $z=2d_1+2d_2$ to $z=2d_1+4d_2$. The field at the plane $z=2d_1+4d_2$ is the FRFT of order $5\pi/4$ of the field at the exit face of the crystal. Lens L_5 is used to perform a $\frac{3\pi}{4}$ FRFT and L_4 was used to perform a $\pi/4$ order FRFT. By choosing different detector positions and combinations of lenses, we could implement several different FRFT's on each down-converted field.

A sample of the experimental results is shown in Fig. 6, which displays coincidence counts $C_{\alpha,\beta}(\rho_1,\rho_2)$ as a function of the dimensionless coordinate ρ_2. In all of the plots, the slit of detector 1 is fixed at the origin ($\rho_1=0$). These figures correspond to vertical cross sections along the line $\rho_1=0$ of the theoretical density plots in Figs. 2 and 3. One can see that for the cases $\alpha+\beta=\pi,2\pi$, a narrow coincidence distribution is observed, indicating either an intensity correlation or anticorrelation. When $\alpha+\beta=3\pi/2$, the coincidence profile is much larger, indicating a much weaker correlation. Using Eq. (23), the conditional variances $\Delta^2_{\alpha,\beta}(\rho_2|\rho_1)$ were determined through Gaussian curve fits of the coincidence distributions. Similar measurements and analysis were conducted by scanning ρ_1 and fixing detector 2 at $\rho_2=0$. The dimensionless variances for all results obtained are presented in Table I. We note that the variance for the weakly correlated distributions is about 10–50 times larger than the correlated and anticorrelated distributions.

The coincidence distribution $C_{\pi/4,3\pi/4}(\rho_1,\rho_2)$ in fact corresponds to the transverse wave-vector distribution $C_{3\pi/4,5\pi/4}(q_1,q_2)$, since the $\alpha=\pi/4(\beta=3\pi/4)$ FRFT differs from the $\alpha=3\pi/4(\beta=5\pi/4)$ FRFT by a Fourier transform. Thus, with the experimental results shown in Fig. 6, we can calculate the EPR inequality (1),

$$\Delta^2_{3\pi/4,5\pi/4}(\rho_1|\rho_2)\Delta^2_{3\pi/4,5\pi/4}(q_1|q_2)=0.039\ 1<\frac{1}{4}, \quad (26)$$

indicating EPR's nonlocality. Similarly, the conditional variances $\Delta^2_{\alpha,\beta}(\rho_1|\rho_2)$ give

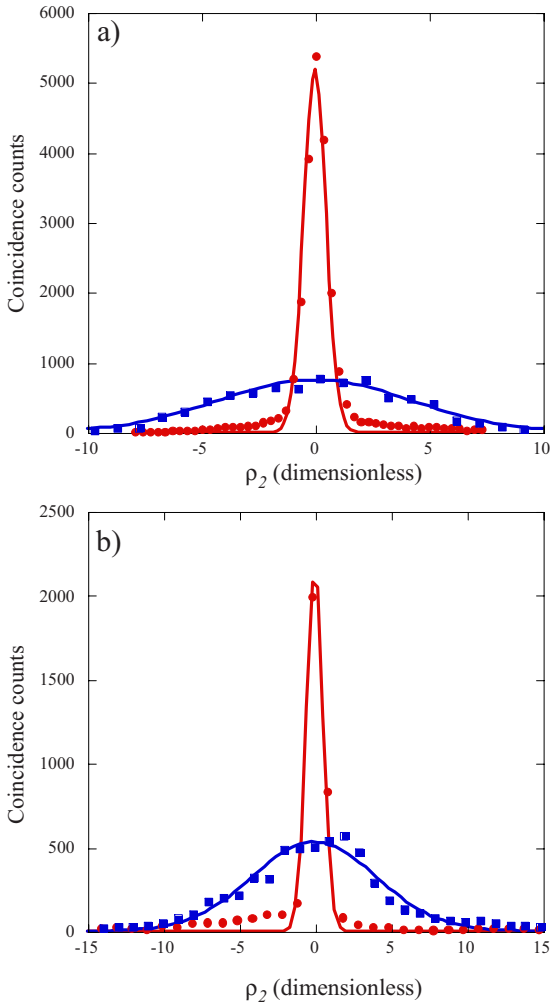

FIG. 6. (Color online) Coincidence counts $C_{\alpha,\beta}(\rho_1,\rho_2)$ as a function of dimensionless ρ_2 for (a) $\alpha=\pi/4,\beta=3\pi/4$ (red circles) and $\alpha=3\pi/4,\beta=3\pi/4$ (blue squares) and (b) $\alpha=3\pi/4,\beta=5\pi/4$ (red circles) and $\alpha=\pi/4,\beta=5\pi/4$ (blue squares). In all cases, detector 1 is fixed at $\rho_1=0$.

$$\Delta^2_{3\pi/4,5\pi/4}(\rho_2|\rho_1)\Delta^2_{3\pi/4,5\pi/4}(q_2|q_1)=0.035\ 2<\frac{1}{4}. \quad (27)$$

It is clear that the EPR intensity correlation is lost when $\alpha+\beta=3\pi/2$, since

$$\Delta^2_{3\pi/4,3\pi/4}(\rho_1|\rho_2)\Delta^2_{3\pi/4,3\pi/4}(q_1|q_2)=244\pm26>\frac{1}{4}, \quad (28)$$

$$\Delta^2_{\pi,\pi}(\rho_2|\rho_1)\Delta^2_{\pi,\pi}(q_2|q_1)=111\pm13>\frac{1}{4}. \quad (29)$$

The results summarized in Table I show the strength but do not indicate the type of correlation. To investigate the type of spatial correlation in intermediate FRFT planes, we first used lens configurations with FRFT orders $\alpha=\frac{5\pi}{4}$ and $\beta=\frac{3\pi}{4}$, satisfying $\alpha+\beta=2\pi$. Experimental results are shown in Fig. 7(a). Initially, the slit in front of detector 1 was placed at the origin ($\rho_1=0$) and the slit in front of detector 2 was scanned vertically. The measured coincidence counts are

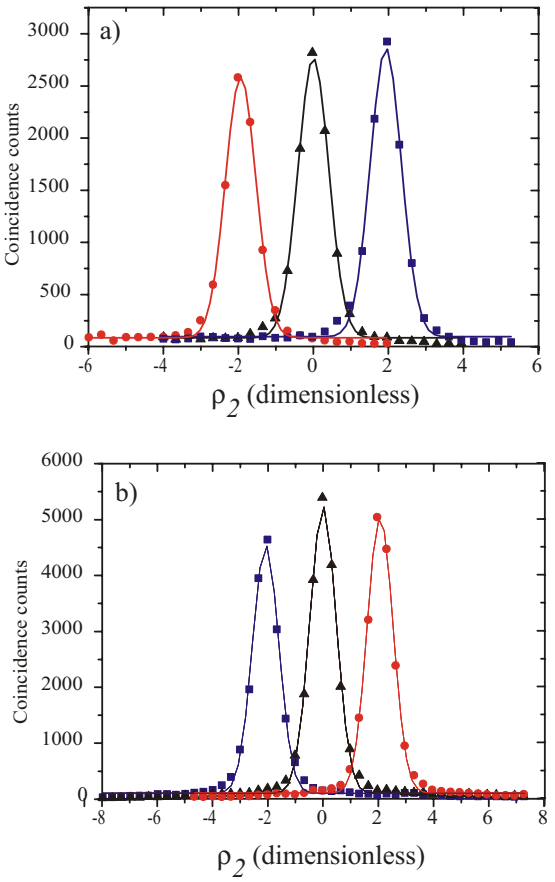

FIG. 7. (Color online) Coincidence counts $C_{\alpha,\beta}(\rho_1,\rho_2)$ as a function of dimensionless ρ_2 for (a) $\alpha=3\pi/4$ and $\beta=5\pi/4$ and (b) $\alpha=\pi/4$ and $\beta=3\pi/4$. In both figures, the black triangles correspond to $\rho_1=0$, the red circles to $\rho_1=-1.99\pm0.03$, and the blue squares to $\rho_1=1.99\pm0.03$. (a) thus shows a correlation, while (b) shows an anticorrelation of the detection positions.

plotted in black triangles in Fig. 7(a) and the maximum of the Gaussian fit is at $\rho_1=0\pm0.03$. We then displaced one of the slits by 300 ± 5 μm, which corresponds to a dimensionless displacement of $\rho_1=1.99\pm0.03$. Coincidence counts were again measured while the slit of detector 2 was scanned. Coincidence counts are in blue squares in Fig. 7(a) and the maximum of the Gaussian fit is at $\rho_2=1.93\pm0.03$. Slit 1 was then moved -300 ± 5 μm ($\rho_1=-1.99\pm0.03$), and slit 2 was scanned. The maximum of the coincidence counts occurred at $\rho_2=-1.94\pm0.03$. We thus observe a strong correlation between the transverse coordinates for this configuration satisfying $\alpha+\beta=2\pi$. The same procedure was performed for the lens configuration $\{\alpha=\frac{3\pi}{4},\beta=\frac{\pi}{4}\}$, which satisfies the anticorrelation condition $\alpha+\beta=\pi$. The results are shown in Fig. 7(b). We observe similar displacement of the coincidence peaks; however in this case the maxima of the Gaussian fits are anticorrelated with the position of the slit of the other detector.

V. CONCLUSION

We have used the fractional Fourier transform to study the propagation of the transverse intensity correlations of the two-photon state produced from parametric down-conversion. The transforms were implemented with simple lens systems. Our theoretical and experimental results show that the propagation of the transverse correlations of highly correlated two-photon states depends upon the sum of the transform orders of the down-converted fields. For $\alpha+\beta=0(\mathrm{mod}\,2\pi)$, the original intensity correlation at the source is recovered, while for $\alpha+\beta=\pi(\mathrm{mod}\,2\pi)$, an intensity anticorrelation is observed. For $\alpha+\beta=\pi/2(\mathrm{mod}\,2\pi)$ or $\alpha+\beta=3\pi/2(\mathrm{mod}\,2\pi)$, almost no correlation is present. Analytical results were obtained for the propagation of the ideal EPR state and numerical calculations along with our experimental results show that the down-converted photons display a similar behavior. The EPR correlation present in the two-photon state was confirmed for several different orders of the fractional Fourier transforms through the violation of an inequality. These results apply to spatially correlated photons obtained from any source, as well as correlations present in other physical systems, and should be useful for engineering spatial correlations, as well as fundamental studies of quantum nonlocality and entanglement.

ACKNOWLEDGMENTS

We would like to thank A. Salles for fruitful discussions. Financial support was provided by Brazilian agencies CNPq, PRONEX, CAPES, FAPERJ, FUJB, and the Millennium Institute for Quantum Information.

[1] A. Einstein, D. Podolsky, and N. Rosen, Phys. Rev. **47**, 777 (1935).
[2] Z. Y. Ou, S. F. Pereira, H. J. Kimble, and K. C. Peng, Phys. Rev. Lett. **68**, 3663 (1992).
[3] C. Silberhorn, P. K. Lam, O. Weiß, F. König, N. Korolkova, and G. Leuchs, Phys. Rev. Lett. **86**, 4267 (2001).
[4] A. S. Villar, L. S. Cruz, K. N. Cassemiro, M. Martinelli, and P. Nussenzveig, Phys. Rev. Lett. **95**, 243603 (2005).
[5] Y. Takeno, M. Yukawa, H. Yonezawa, and A. Furusawa, Opt. Express **15**, 4321 (2007).
[6] J. C. Howell, R. S. Bennink, S. J. Bentley, and R. W. Boyd, Phys. Rev. Lett. **92**, 210403 (2004).
[7] M. D'Angelo, Y.-H. Kim, S. P. Kulik, and Y. Shih, Phys. Rev. Lett. **92**, 233601 (2004).
[8] B. Julsgaard, A. Kozhekin, and E. S. Polzik, Nature (London) **413**, 400 (2001).
[9] W. P. Bowen, N. Treps, R. Schnabel, and P. K. Lam, Phys. Rev. Lett. **89**, 253601 (2002).
[10] W. P. Bowen, R. Schnabel, Hans-A. Bachor, and P. K. Lam, Phys. Rev. Lett. **88**, 093601 (2002).
[11] M. V. Fedorov, M. A. Efremov, A. E. Kazakov, K. W. Chan, C. K. Law, and J. H. Eberly, Phys. Rev. A **72**, 032110 (2005).

[12] S. L. Braunstein and P. van Loock, Rev. Mod. Phys. **77**, 513 (2005).
[13] H. Bechmann-Pasquinucci and W. Tittel, Phys. Rev. A **61**, 062308 (2000).
[14] M. Bourennane, A. Karlsson, and G. Bjork, Phys. Rev. A **64**, 012306 (2001).
[15] D. Collins, N. Gisin, N. Linden, S. Massar, and S. Popescu, Phys. Rev. Lett. **88**, 040404 (2002).
[16] M. D. Reid and P. D. Drummond, Phys. Rev. Lett. **60**, 2731 (1988).
[17] M. D. Reid, P. D. Drummond, E. G. Cavalcanti, W. P. Bowen, P. K. Lam, H. A. Bachor, U. L. Andersen, and G. Leuchs, e-print arXiv:0806.0270, Rev. Mod. Phys. (to be published).
[18] L.-M. Duan, G. Giedke, J. I. Cirac, and P. Zoller, Phys. Rev. Lett. **84**, 2722 (2000).
[19] S. Mancini, V. Giovannetti, D. Vitali, and P. Tombesi, Phys. Rev. Lett. **88**, 120401 (2002).
[20] D. V. Strekalov, A. V. Sergienko, D. N. Klyshko, and Y. H. Shih, Phys. Rev. Lett. **74**, 3600 (1995).
[21] P. H. S. Ribeiro, S. Padua, J. C. Machado da Silva, and G. A. Barbosa, Phys. Rev. A **49**, 4176 (1994).
[22] T. B. Pittman, D. V. Strekalov, D. N. Klyshko, M. H. Rubin, A. V. Sergienko, and Y. H. Shih, Phys. Rev. A **53**, 2804 (1996).
[23] C. H. Monken, P. H. Souto Ribeiro, and S. Padua, Phys. Rev. A **57**, 3123 (1998).
[24] A. F. Abouraddy, B. E. A. Saleh, A. V. Sergienko, and M. C. Teich, Phys. Rev. Lett. **87**, 123602 (2001).
[25] J. P. Torres, Y. Deyanova, L. Torner, and G. Molina-Terriza, Phys. Rev. A **67**, 052313 (2003).
[26] T. Yarnall, A. F. Abouraddy, B. E. A. Saleh, and M. C. Teich, Phys. Rev. Lett. **99**, 170408 (2007).
[27] M. P. Almeida, S. P. Walborn, and P. H. Souto Ribeiro, Phys. Rev. A **72**, 022313 (2005).
[28] K. W. Chan, J. P. Torres, and J. H. Eberly, Phys. Rev. A **75**, 050101(R) (2007).
[29] D. S. Tasca, S. P. Walborn, P. H. Souto Ribeiro, and F. Toscano, Phys. Rev. A **78**, 010304(R) (2008).
[30] H. M. Ozaktas, Z. Zalevsky, and M. A. Kutay, *The Fractional Fourier Transform: With Applications in Optics and Signal Processing* (Wiley, New York, 2001).
[31] T. Alieva, V. Lopez, V. Agullo-Lopez, and L. B. Almeida, J. Mod. Opt. **41**, 1037 (1994).
[32] P. Pellat-Finet, Opt. Lett. **19**, 1388 (1994).
[33] P. Pellat-Finet and G. Bonnet, Opt. Commun. **111**, 141 (1994).
[34] A. W. Lohmann, J. Opt. Soc. Am. A **10**, 2181 (1993).
[35] D. Marcuse, *Light Transmission Optics* (Van Nostrand Reinhold, New York, 1982).
[36] Note that in the paraxial approximation, the transverse components of the wave vector $\vec{k}$ are $q_l \approx k\theta_l$ ($l=x,y$ and $k \equiv |\vec{k}| = 2\pi/\lambda$) where $\theta_l \ll 2\pi$ are the angles between $\vec{k}$ and the z axis. Thus, considering $\lambda/2\pi$ analogous to $\hbar$, we can write $[\hat{\rho}_k, \hat{\theta}_l] = i(\lambda/2\pi)\delta_{k,l}$ or $[\hat{\rho}_k, \hat{q}_l] = i\delta_{k,l}$.
[37] D. Stoler, J. Opt. Soc. Am. **71**, 334 (1981).
[38] D. Gloge and D. Marcuse, J. Opt. Soc. Am. **59**, 1629 (1969).
[39] H. Bacry and M. Cadilhac, Phys. Rev. A **23**, 2533 (1981).
[40] D. Dragoman, Prog. Opt. **42**, 424 (2002).
[41] C. I. Osorio, S. Barreiro, M. W. Mitchell, and J. P. Torres, Phys. Rev. A **78**, 052301 (2008).
[42] C. I. Osorio, A. Valencia, and J. P. Torres, New J. Phys. **10**, 113012 (2008).
[43] S. P. Walborn, A. N. de Oliveira, S. Pádua, and C. H. Monken, Phys. Rev. Lett. **90**, 143601 (2003).
[44] L. Mandel and E. Wolf, *Optical Coherence and Quantum Optics* (Cambridge University Press, New York, 1995).